Design and Development of a Rose Plant Disease-Detection and Site-Specific Spraying System based on a Combination of Infrared and Visible Images

S. Minaei[1], M. Jafari[1]*, and N. Safaie[2]

ABSTRACT

Rose, as one of the oldest flowers in cultivation and the most popular of all cut flowers throughout the world, is susceptible to several diseases. Powdery mildew and gray mold are two of the most common diseases in the greenhouse cultivation of roses. Changes in plant leaf temperature mainly resulting from changes in transpiration in response to such stresses as pathogen infection, water stress, or physiological changes can be monitored instantly and remotely by thermographic imaging. In this research, a smart detection and spraying system was designed and developed to recognize rose powdery mildew and gray mold diseases using a combination of thermal and visible images. The system consists of a thermal camera and a visual camera both mounted on a C-shaped carriage. The carriage is capable of moving along plant rows and rotating around each rose shrub. In addition, a site-specific sprayer was designed that consisted of an electrically-actuated pneumatic directional valve, a pneumatically-actuated directional valve, a pressure regulator, a pressure tank, a compressor, a manual flow control valve, and a nozzle. Droplets volume median diameter, percent of coverage, and system performance in spraying the specified positions were evaluated. Analysis of the pre- and post-spray thermal images showed that such index as temperature median can be successfully exploited to determine spray coverage and uniformity.

Keywords: Image registration, Percent of coverage, Thermal histogram, Volume median diameter.

INTRODUCTION

The application of pesticide is still one of the most frequently used methods of plant protection against diseases and insects in agriculture (Mostafaei Maynagh *et al.*, 2009). In this regard, the environmental protection regulations were established to eliminate or reduce exposure to pesticides, and to inform the spraying personnel of the potential hazards associated with pesticide spraying. In most agricultural applications, these regulations require protective suits and face masks to be worn by farmers when spraying pesticides. Although these provisions provide workers with some protection, they have the disadvantage of giving an uneasy feeling of discomfort or being in a dangerous situation because of the high temperature inside the suit which might run the risk of serious dehydration. Most of the associated hazard and discomfort may be eliminated by using automated systems of pesticide application instead of the commonly used manual ones (Rowe *et al.*, 2000).

_____

[1] Department of Biosystems Engineering, Faculty of Agriculture, Tarbiat Modares University, Tehran, Islamic Republic of Iran.

[2] Department of Plant Pathology, Faculty of Agriculture, Tarbiat Modares University, Tehran, Islamic Republic of Iran.

*Corresponding author; email: mehrnoosh.jafari@modares.ac.ir

In current agricultural practice, pesticides are uniformly applied throughout the field according to a schedule that is rarely prepared based on expert recommendations (Oberti *et al*., 2014). Moreover, while disease symptoms can be detected by plant pathologists or experienced practitioners, such experts may not always be available on all farms. Hence, an accurate, fast, automatic, and targeted system is needed as a substitute for such unavailable expert diagnosis (Polder *et al*., 2014). Such a system is additionally capable of early detection of symptoms and proper selection of a meaningful diseased-plant treatment that prevents the spread of the disease and reduces farmer losses (Oberti *et al*., 2014). The approach commonly recommended by researchers is the use of machine vision as a novel sensor-based method for disease detection that can be used in precision agriculture, crop protection (Rumpf *et al*., 2010), and disease detection in open fields (Sankaran *et al*., 2010b).

Many research efforts have so far been directed toward the use of smart non-invasive techniques to identify diseases and nutritional deficiencies in plants, capable of recognizing on-field plant pathogens with no damage to plant tissues or leaves. Imaging and spectroscopic methods are two such disease monitoring techniques (Sankaran *et al*., 2010a).

Currently, high resolution cameras are available that mainly use broad band RGB color or Near-Infrared (NIR) sensors, multispectral sensors using 4 to 10 wavelength bands, hyperspectral sensors with up to 300 narrow wavelength bands (Polder *et al*., 2014), or long-wave-infrared sensors that convert the invisible thermal radiations from an object into visual images (Vadivambal and Jayas, 2011).

Other spectroscopic and imaging techniques employed for the detection of symptomatic and asymptomatic plant diseases include fluorescence spectroscopy (Marcassa *et al*., 2006; Belasque *et al*., 2008; Lins *et al*., 2009), fluorescence imaging (Bravo *et al*., 2003; Moshou *et al*.,

2005; Chaerle *et al*., 2007), infrared spectroscopy (Spinelli *et al*., 2006; Purcell *et al*., 2009), multispectral and hyperspectral imaging (Moshou *et al*., 2004; Shafri and Hamdan, 2009; Qin *et al*., 2009); and thermal imaging (Stoll *et al*., 2008; Lindenthal *et al*., 2005; Oerke *et al*., 2006; Oerke *et al*., 2011; Wang *et al*., 2012, Chaerle *et al*., 1999).

Thermal imaging is a thermographic method that uses infrared radiation to form pseudo-images. The devices used in this method convert thermal infrared radiation emitted by objects into thermal data without the need for any direct contact with the plant. Using thermal imaging to identify diseased plants is based on the hypotheses that diseases affect plant transpiration and respiration rates and that pathogenic infection can result in significant changes in leaf temperature. However, the challenge in the use of thermal images to distinguish infected plants from non-infected ones lies in the fact that plant temperature is also affected by both biotic and abiotic stresses (Oerke *et al*., 2006).

Roses are commercially important cut flowers with more than 130 species belonging to the Rosaceae family. They are susceptible to a number of diseases whose early detection and control may help avoid economic losses. Caused by the obligate biotroph "*Podosphaerapannosa*", powdery mildew may be the most common disease among greenhouse, garden, and field-grown roses. Severe damage to infected flowers affects their visual appeal, and thereby their commercial value (Horst, 1983; Linde and Shishkoff, 2003).

Botrytis cinerea Pers. is a ubiquitous fungal pathogen that causes gray mold not only in many fruits but also in vegetable and ornamental crops, thereby posing a major challenge to greenhouse producers worldwide (Macnish *et al*., 2010) especially high-value flowers. Chemical pesticides have for long been used as the first line of defense against fungal diseases. However, the use of pesticides is problematic due to

the growing environmental concerns over chemical residues and worker exposure.

The demand for rose flowers during all the four seasons of the year has led to the cultivation of roses under greenhouse conditions in which pesticides form an important tool to manage diseases. However, their application in enclosed spaces increases the risk of worker exposure. In this regard, smart detecting and spraying systems offer a number of benefits that justify their application. These include: controlling diseases in the early stages of pathogenesis which leads to their restricted spread, reduced exposure to the spray materials, reduced application rates, eliminated variability associated with hand-spraying, greater repeatability and accuracy, and less disruption to other greenhouse labor operations. Based on these considerations, the present study was conducted to design, develop, and evaluate an automatic detecting and spraying system based on the use of thermal images.

MATERIALS AND METHODS

Thermal Camera

Digital thermal images were taken using a non-cooled focal-plane-array infrared camera (ITI-P400, ITI Infrared AB, Sweden). The instrument operates in a waveband range of 8–14 μm and is capable of measuring temperatures in the range of –20 to 250°C. The detector array has a geometric resolution of 25 μm (384×288 pixels focal plane array) and a 21.7°×16.4° field view lens with a minimum focus distance of 0.3 m.

The camera used enjoys a thermal resolution of 0.08°C and an absolute temperature measurement accuracy of less than ±2°C. It is important to note that the crucial data used for the diagnostic work is the relative temperatures of different points on the interested area. Hence, camera resolution is of utmost importance. Emissivity was fixed at 0.98 throughout the entire experiment. The thermal images were initially extracted and analyzed using the ITI IrAnalyser (ITI Infrared AB., Sweden) software.

Visual Camera

Visible images were captured using a digital camera (Canon 550D Kiss X4, Canon Inc., Japan) with the remote shooting capability. The camera was connected to a PC *via* the USB cable. Image capturing and some of the camera adjustments were accomplished using a Zoom Browser Ex. 6.7. Images, 5,184×3,456 pixels, were saved in compressed and raw formats.

Design of the Moving Carriage

A two-degrees-of-freedom automatic image capturing system was designed with the capability both to move along plant rows and to rotate around each rose shrub (Figure 1).One DC motor was mounted for each moving axis (12VDC,40W) (Ruian Rizen Auto parts Co., China). A rack and pinion mechanism was used as a linear actuator to move along the longitudinal axis and a 360 pulse digital optical encoder was utilized to convert its motion into a sequence of digital pulses. The Cameras were mounted on a *C*-shaped carriage that was constructed using an aluminum linear guideway formed by a rolling mill. The linear guideway carriage travels the rail with a wire rope and a pulley. An encoder was used to determine the DC motor angular position. The base of the set-up was constructed using hollow cross section aluminum profiles 60×60 mm in size. A height-adjustable automatic image capturing set-up was achieved by using special fasteners to mount these profiles.

Design of the Site-Specific Sprayer

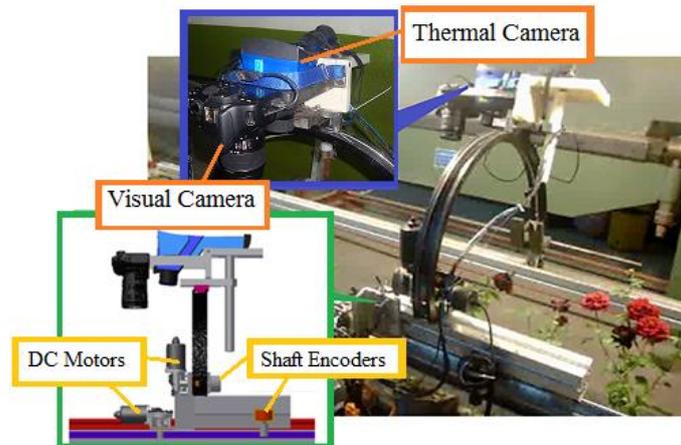The major components of the site-specific spraying system include a pressurized

Figure 1. The developed automatic image capturing set-up.

pesticide tank with a capacity of 16.7 L that is rated at a maximum pressure of 1.75×10^6 Pa, a pressurized air source (a compressor), an electrically-actuated pneumatic directional valve, a pneumatically-actuated pneumatic directional valve, a pressure regulator, a manual flow control valve, and a nozzle. The schematic diagram and photograph of the site-specific sprayer are shown in Figure 2.

When the nozzle reaches the desired position, the electrically-actuated directional valve is activated by the PLC output. Thus, air will flow into the pneumatically-actuated pneumatic directional valve which directs pressurized pesticide into the nozzle. As soon as the nozzle passes the spray zone, the PLC turns off the output and the spring returns the electrically-actuated directional

valve to its original (OFF) position (Figure 2).

The nozzle tip is one of the most important and least expensive parts of the spraying system. Nozzles are used to break up the liquid into droplets and to form the spray pattern. They additionally determine the application volume at a given operating pressure. The drift can be minimized by selecting nozzles that produce the largest droplet size while also providing adequate coverage at the intended application rate and pressure. The most common type of nozzle used in agriculture is the fan nozzle which is widely used for spraying pesticides—in both banding (over and between rows) and broadcast applications.

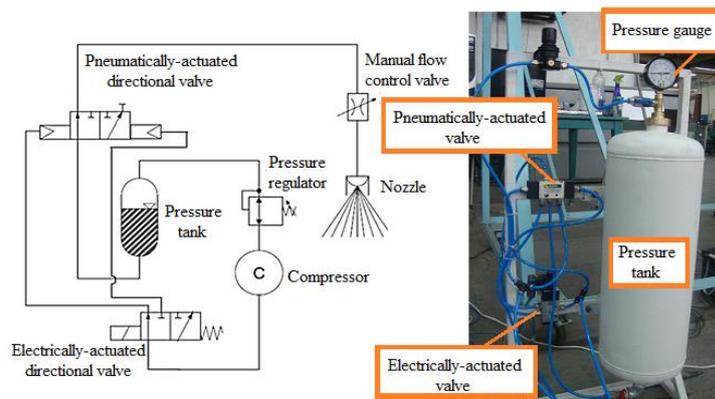Given the type of spraying (banding) required in this study and the limited market

Figure 2. Schematic diagram and photograph of the site-specific sprayer.

availability of nozzles, a flat fan nozzle was selected for the purpose. Experimental results showed that thorough covering of nine rose plant pots with fungicide, while the pots were placed on a 3m-long row, required 300 mL of fungicide. Based on the experimental results obtained, the fungicide application rate was calculated to be 1,000 L ha^{-1}.

In general, agricultural statistical surveys have indicated that pesticides are usually applied at the following rates:

Herbicides are sprayed in orchards and vineyards in 150 to 600 L of water per hectare.

Insecticides and fungicides are sprayed in 500 to 1,000 L of water per hectare for boom sprayers, anywhere from 500 L to 2,000 L per hectare for orchards, and 500 L to 1,000 L per hectare for vineyards.

Aerial applications may use lower application rates; for example, from 25 to 400 L per hectare.

The amounts of herbicides and fungicides sprayed in most large-scale Iranian greenhouses producing roses are in the range of 500 to 700 L per hectare. This is while application rates in traditional cultivations may reach as high as 5 times the above rates. It should be noted that in the rose greenhouses, even higher rates of pesticide application do not guarantee effective distribution due to the difficulty of moving between adjacent rows.

To select the proper nozzle size, the forward speed of the system was calculated. Measurements showed that the DC motor was able to travel a distance of 3.05 m at 40 seconds. Hence, the forward speed of the system was calculated to be 0.27 km h^{-1}.

Taking into account the travel speed (0.27 km h^{-1}), the spray application rate (1,000 L ha^{-1}), and the nozzle spacing (1 m), the nozzle spraying rate was estimated as 0.45 L min^{-1}.

Based on the obtained nozzle rate (0.45 L min^{-1}) and a working pressure of 2×10^5 Pa, a Teejet 110015 nozzle was selected. Nozzle height was subsequently changed to 65 cm above the ground in order to adjust the effective spray width of one meter (width of the plant row).

Electrical Structure of the System

The electrical structure of the designed system consisted of two encoders to measure the displacement and angular position of the camera holder, two DC motors, an electrically-actuated directional valve, and a PLC (Figure 3). In this study, a FATEK-
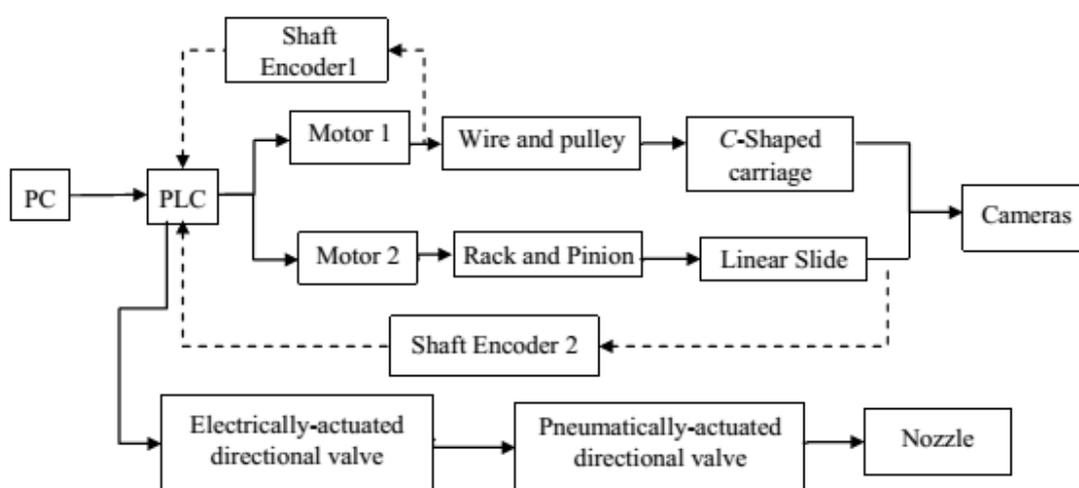

Figure 3. Block diagram of the machine vision and smart spraying system.

FBs-20MAT/J PLC (FATEK Automation Corporation, Taiwan) was used to provide communication between the software and the hardware components of the system. The PLC was connected to the PC via a RS232 serial port and a ladder control program was written using the FATEK-FBs-PLC Winproladder software.

A switching power supply of 180W (12V and 15A) was utilized to provide power to the DC motors. In the control circuit of the system, each DC motor was controlled by two contactors (Figure 4).

Graphical User Interface Software

The graphical user interface software was written in LabVIEW which made the following four operations available to the user:

1. The ability to manually change the position on each axis in the "Manual Movement" frame.

2. Calibration of the sprayer in the "Sprayer calibration" frame.

3. Automatic movement of the imaging set-up in the "Automatic Movement" frame.

4. Map-based automatic spraying –by inserting a spraying map in the form of a two-dimensional matrix in the "Automatic spraying" frame (Figure 5).
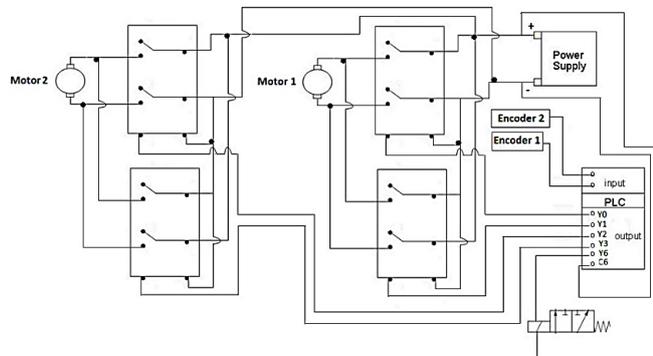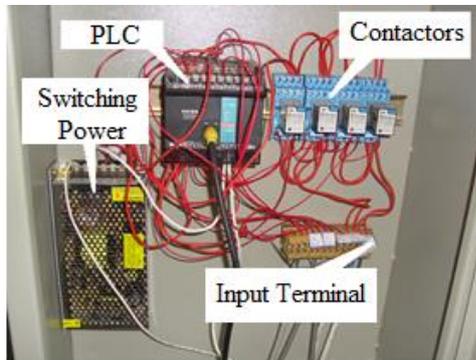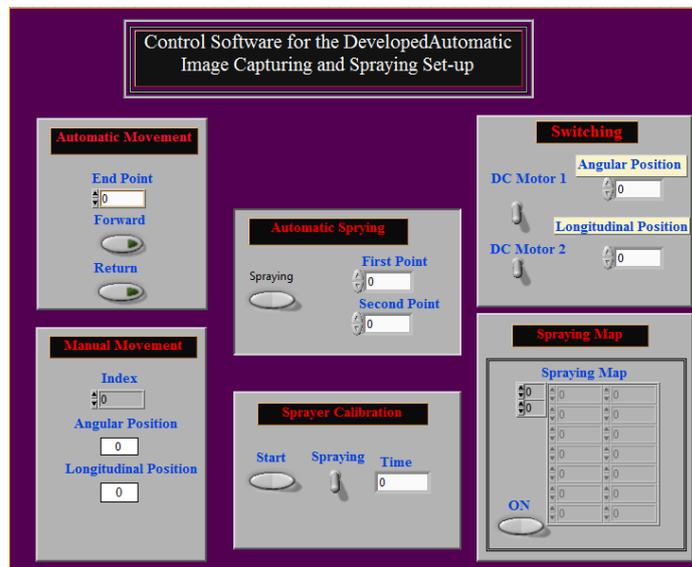

Figure 4. Electrical control circuit of the system.

Figure 5. The designed graphical user interface software.

Image Processing

Feature detection is difficult or even impossible in thermal images due to their low contrast. It is, therefore, essential to utilize visual images instead since objects can then be recognized based on their color, dimensions, and other visual properties.

To simplify image registration, thermal and visual cameras were installed in a line in front of each other. Automatically captured thermal and visible images were pre-registered with the use of a designed checkerd surface. Then, an intensity-based automatic image registration method was utilized to successfully register the pre-registered thermal images with the corresponding visible images (Figure 6).

Different segmentation algorithms were examined to recognize leaves and flowers accurately. The segmented pictures were next utilized as a mask to separate the desired parts of the corresponding thermal image (Figure 7). Then, thermal histograms and thermal features of each picture were extracted.
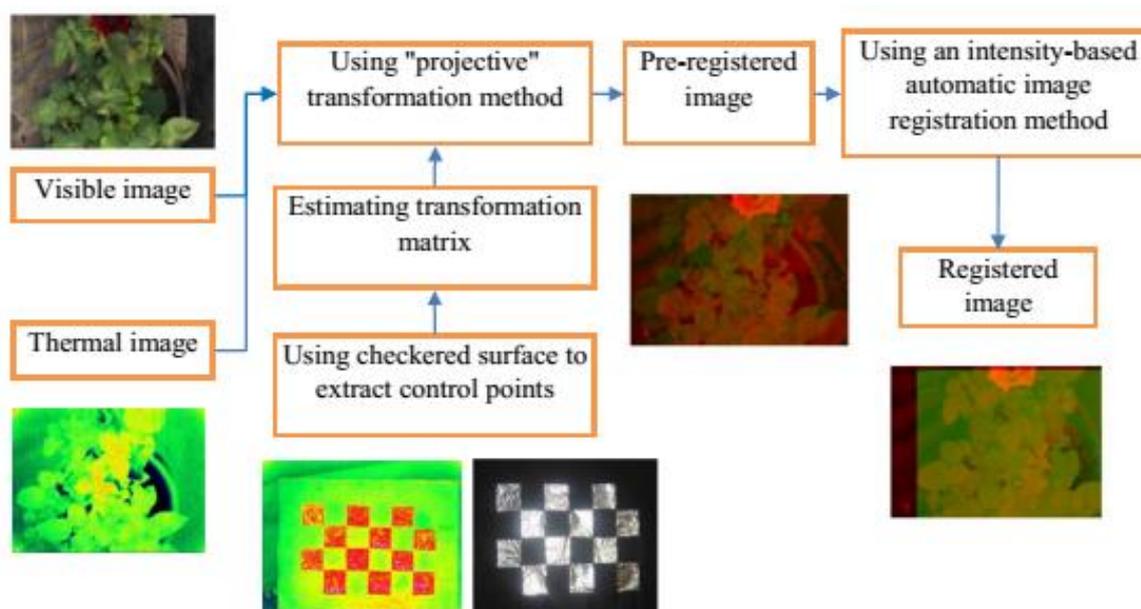

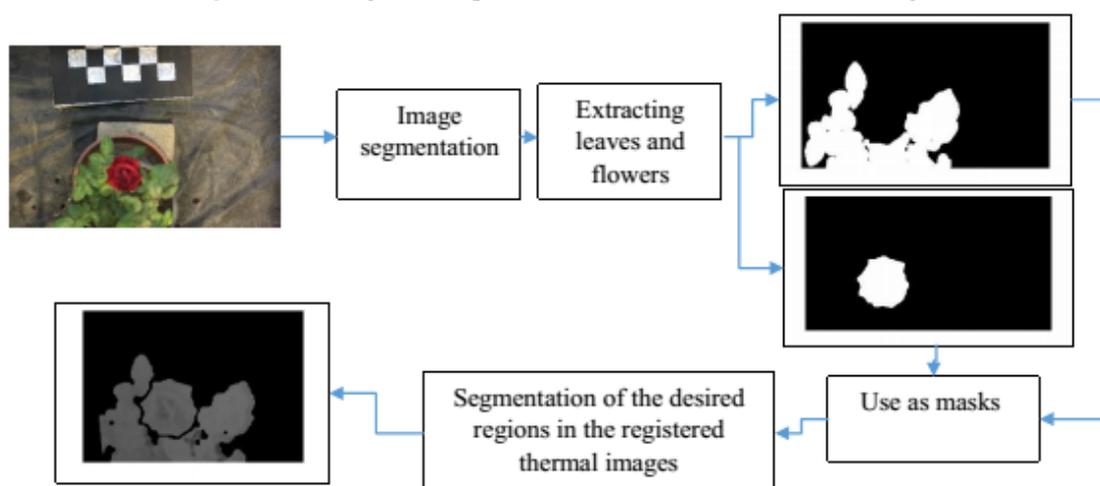**Figure 6.** The registration procedure of the thermal and visible images.

Figure 7. Segmentation algorithm for the thermal images.

Sprayer Calibration

To prevent irregular and excessive spraying, the sprayer was calibrated. In order to save on pesticide consumption, to prevent plant burning, and to avoid undesirable environmental contamination, water was used in the calibration process. For this purpose, regulator pressure was set to 2×10^5 Pa and the sprayer tank was filled with 9 liters of water. It should be noted that the spraying rate increases and the droplet size decreases with increasing the working pressure.

The total spray output of the machine was measured in order to apply a specified rate of chemical spray onto the target surface, e.g. plant, soil, and pest. For this purpose, the spraying rate was calibrated by measuring the nozzle output using a graduated cylinder and calculating the elapsed time using an especially written code. The manual flow control valve was then adjusted to set the nozzle output to 1,000 L ha^{-1}.

Sprayer Evaluation

The sprayer calibration and proper selection of nozzle size require the distribution pattern and droplet size to be determined in advance. A number of methods and different theories have been proposed for this purpose. One of the most practical and cost-effective methods commonly used is the water sensitive paper, which is a paper coated with the chemical indicator Bromophenol Blue. The paper is yellow and will turn blue when it comes in contact with the falling droplets. Spray droplets stain the water sensitive paper coating and the resulting spot sizes can be assessed through an image processing method (Sayıncı *et al*., 2012).The parameters that can be extracted from water sensitive papers include: number of impacts per unit area, percent coverage, equivalent diameter for each impact (assuming that the impacts have a circular shape), Volume Median Diameter (VMD), Number Median Diameters (NMD), spray quality parameter, and relative span factor (Maghsoudi *et al*., 2015). The ImageJ 1.49v software (developed by the National Institutes of Health, USA) was used for the acquisition, analysis, and processing of water sensitive paper images.

Two different procedures were designed and implemented to evaluate the quality and accuracy of the site-specific sprayer. In the first, eight pots of rose plants were placed at regular spaces along a row 3 m in length and 1 m in width. Then, two water sensitive papers were placed on the upper leaves of each rose plant and the same number of water sensitive papers were pasted on the lower leaves. The nozzle sprayer was operated to spray the plants at a constant pre-defined rate (1,000 L ha^{-1}) and the coverage and distribution patterns were evaluated.

In the second procedure, the response of the site-specific sprayer was examined as a means for sprayer evaluation based on the assumption that the nozzle was able to spray pesticides to a specified distance between 70 and 100 cm from the beginning of the plant row. For this purpose, a thin sheet of foam was laid on the ground on which the water sensitive papers were pasted at a longitudinal distance of 10 cm from the starting point of the plant row (50 to 120 cm). In addition, the transversal spray performance was evaluated by placing three pieces of water sensitive papers in each row at lateral intervals of 25 cm (Figure 8-b).

As using water sensitive papers for sprayer test and calibration is time-consuming and labor-intensive, infrared image analysis was chosen as a potential method for observing pesticide distribution in the plant rows. This was accomplished by passing the thermal and visual cameras above the plant pots before and after the spraying event. The thermal histogram of each image was then extracted and the statistical parameters were calculated.

In this stage of sprayer evaluation, the developed site-specific sprayer was operated

to spray the pesticide uniformly across the plant rows (starting at 100 cm from the beginning of the plant row to its end). Immediately after spraying, thermal and visual images were automatically taken and saved which were then automatically registered and segmented using the selected image processing algorithm. This was followed by plotting the relevant thermal histograms and computing the temperature medians.

RESULTS AND DISCUSSION

Evaluating Uniform Spraying

Adjusting the nozzle output to the high spraying rate of 1,000 L ha^{-1} led to the thorough coverage of the water sensitive papers. Results showed the average coverage values of 95.23 and 69.36% on the upper and lower leaves, respectively. Since leaves overlap, a decrease in percent coverage on the lower water sensitive papers is normally expected.

Evaluating Site-Specific Spraying

As can be seen in Figure 8-b, most of the papers located at points ahead of the specified-zone (specified-zone was 70 to 100 cm) were affected by the nozzle output.

Flat-fan nozzles spray in an inclined pattern in a forward direction. Flat-fan nozzles are, therefore, recommended to be installed at a backward inclination angle of 30°. Figure 8-a shows the longitudinal and lateral coverage percentages computed by the ImageJ software. According to Figure 9, a 100% coverage was achieved at a distance 60 to 80 cm from the starting point of the plant row. The impact diameters of the water sensitive papers used in the uniform spray evaluation experiment were not measurable because of the high application rate of 1,000 L ha^{-1}. At this density, many droplets overlapped and the papers were blue in color. Therefore, the water sensitive papers with low coverage percentages collected from the second experiment i.e., the site-specific spray evaluation, were utilized to estimate the droplet sizes. In this process, the ImageJ software was used and it was found that droplets with smaller Diameters (Dv$_{0.1}$) accounted for 10% of the total volume of the sprayed liquid while those with larger Diameters (Dv$_{0.9}$) accounted for 90% of the total volume of the sprayed liquid (Table 1).

In general, the sprayed droplets were grouped into the following three sizes groups (Moltó *et al.*, 2001):
a) Small droplets: comprising those with an equivalent diameter of less than 200 μm; these evaporate rapidly;
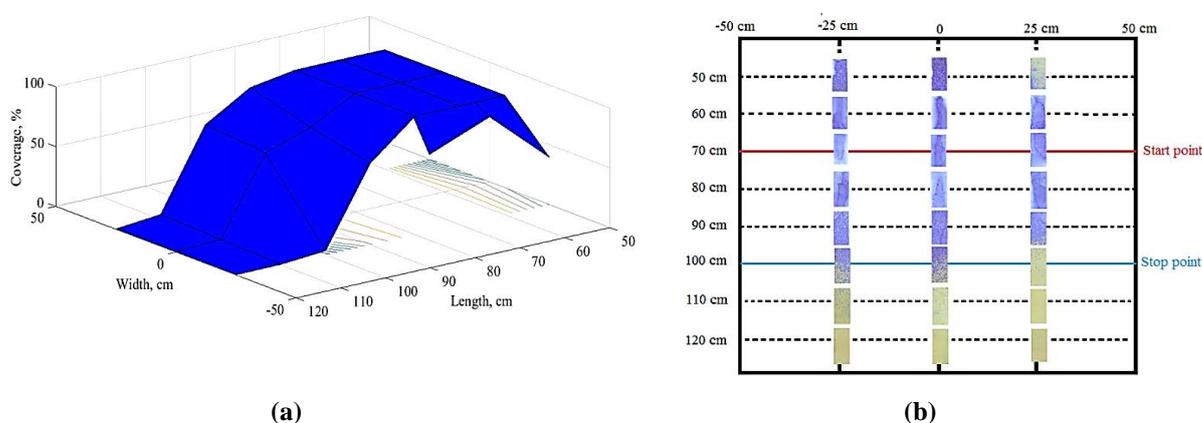b) Medium droplets: those with an

(a)

(b)

Figure 8. (a) Longitudinal and lateral coverage percentages**,** and (b) Arrangement of the water sensitive papers.
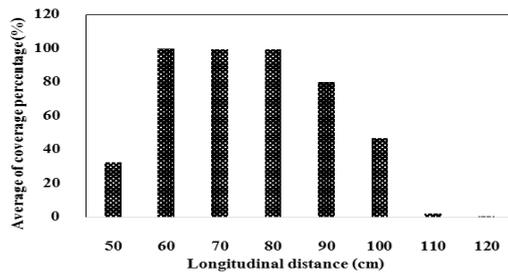
Figure 9. Average of coverage percentage values in the longitudinal direction.

equivalent diameter between 200 and 400 μm; these droplets are conventionally considered as the most effective for ordinary pest control;

c) Large droplets: including those with an equivalent diameter larger than 400 μm.

According to Table 1, only 10% of all the sprayed droplets belonged to the small diameter (smaller than 200 μm) group of droplets. Although small size droplets are easily suspended in the air, these particles will settle on all surfaces in the greenhouse and will not propagate in the surroundings if vents are kept closed and air-circulation is prevented.

One criterion used to judge the efficiency of a spraying operation is the density of spray droplet deposited per unit of leaf area, usually expressed as droplets per cm^2. The recommended ranges for herbicide, fungicide, and insecticide applications are 25 to 30, 50 to 70, and 30 to 40 droplets per cm^2, respectively (Prokop and Kejklicek, 2002). Thus, those water sensitive papers that became thoroughly blue in color represented a state of oversaturation for most of the spray applied.

Based on the recommended values for fungicide application (70 droplets per cm^2)

and given the medium size (200 μm) of the droplets, a simple calculation will indicate that either the speed must be increased from 0.27 to 9 km h^{-1} (a 34-fold increase) or the nozzle type should be changed. In the present case, an atomizer nozzle with a low flow rate of 0.02 L min^{-1} is recommended.

Sprayer Evaluation Using Thermal Images

Figure 10 presents a bar chart of leaf temperature medians before and after spraying. As it is shown in the figure, since the sprayed water was colder than the leaves surfaces, the temperature median decreased after spraying. Also, evaporation of the sprayed water is another cause of the decrease in the plant temperature after spraying. It should be noted that, in this stage of the experiment, to avoid wetting the designed checkered surface, the controlling command was sent to the electrically actuated pneumatic directional valve at the longitudinal distance of 100 cm from the beginning.

Site-Specific Spraying

A distance of 100 to 130 cm from the beginning of the longitudinal moving axis was specified to be sprayed by the developed sprayer. However, as seen in Figure 11, the sprayer affected a wider zone (90 to 130 cm). Figure 12 shows the temperature medians of the thermal histograms. Comparison of Figures 11 and 12 reveals that the positions at 100 and 110 cm from the beginning of the longitudinal moving axis recorded the lowest temperature

Table 1. Droplets size distribution in the spray.

Calculated parameter	Droplet diameter (μm)		
	$Dv_{0.1}$[a]	$Dv_{0.5}$[a]	$Dv_{0.9}$[a]
Average	175	416	707
Standard deviation	70	110	222

[a] $Dv_{0.1}$, $Dv_{0.5}$ and $Dv_{0.9}$: Diameter at which a volume fraction of 10, 50, 90 percent is made up of drops with diameters smaller than this value (μm).
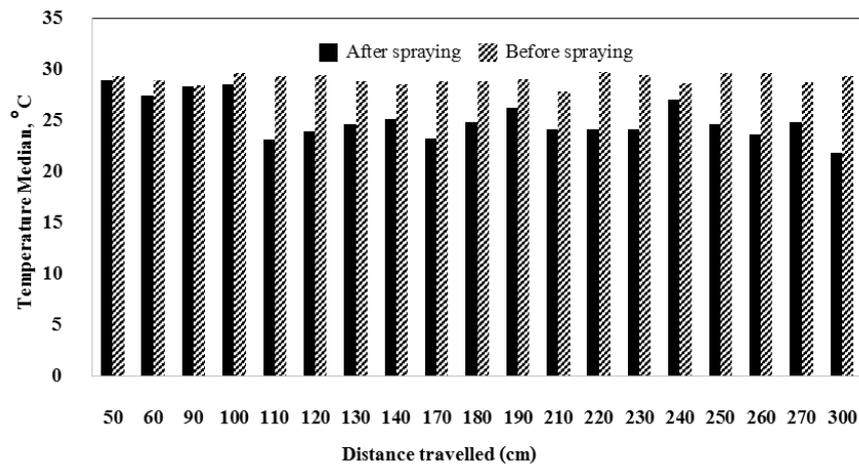
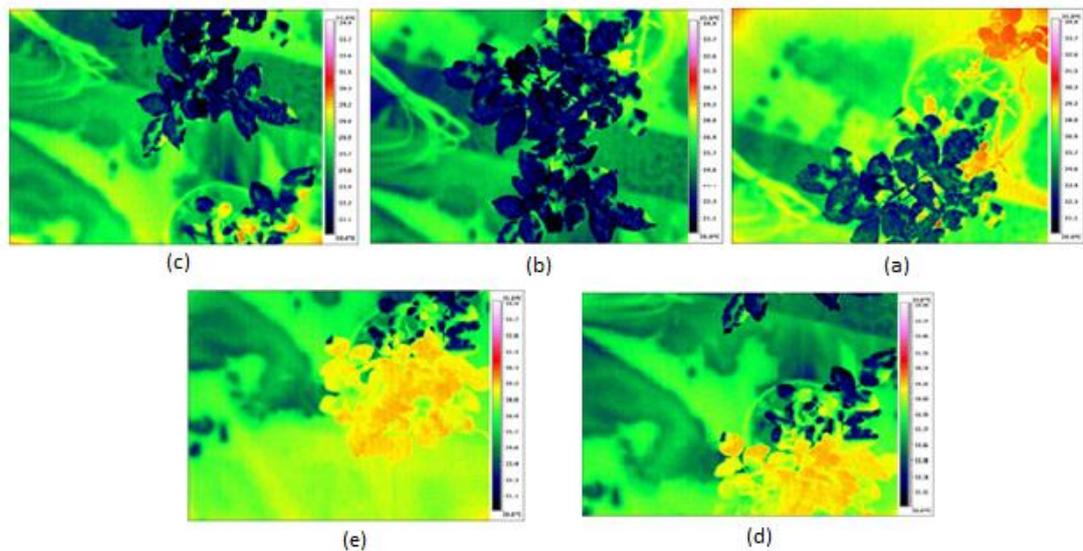**Figure 10**. Temperature median of the leaves before and after spraying.

Figure 11. Thermal images of the specified positions at: (a) 90, (b) 100, (c) 110, (d) 120, and (e) 130 cm from the beginning of the longitudinal moving axis after the spray operation.
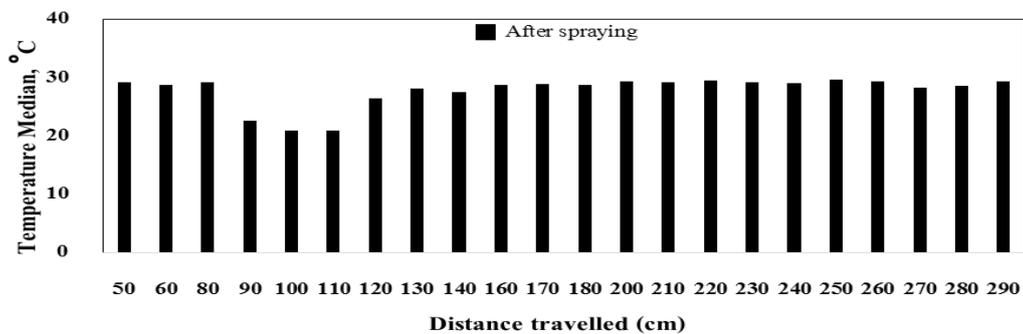

Figure 12. Temperature medians of the leaves from the beginning to the end of the longitudinal moving axis.

medians and the maximum coverage percentages. It may thus be concluded that the measured temperature median is inversely related to the percentage of coverage.

Menessatti *et al*. (2008) were the first and the only one who conducted a feasibility study of assessing spray pattern on hedgerow crops using thermal imagery. In their study, distribution quality was compared with pre-treatment and post-treatment Temperature differences (ΔT) obtained from thermal images. Using the same images, they also compared different sprayer configurations on the vertical axis. Moreover, application of water colder than the leaf surface was considered to make the analysis of thermal images more feasible. *K*-means clustering algorithm was used to segment the resulting (ΔT) images in few grayscale classes. Obviously, existence of more variability in water distribution leads to greater *K* values in the *K*-means clustering algorithm.

In the present ongoing study, the thermal and visual images are employed to determine more valuable features, i.e. distribution uniformity, percentage of coverage, droplets diameters, etc., of the spraying system. Moreover, the site-specific sprayer system designed and manufactured will be evaluated against other types of nozzles and working pressures.

CONCLUSIONS

In this study, a system was designed which was not only capable of moving along plant rows but also rotating around plants. It captures images automatically and performs image segmentation and registration all in one unit. The site-specific sprayer can spray positions that are detected to be diseased-infected. Image processing indicated that temperature median obtained from the thermal images can successfully be exploited to evaluate the performance of a uniform spraying system. However, based

on the efficient values for fungicide application and the ideal size of droplets, increasing forward speed to 9 km h^{-1} or using an atomizer nozzle with a low flow rate of 0.02 L min^{-1} is recommended.

REFERENCES

1. Belasque, L., Gasparoto, M. C. G. and Marcassa, L. G. 2008. Detection of Mechanical and Disease Stresses in Citrus Plants by Fluorescence Spectroscopy. *Appl. Op.,* **47(11):** 1922–1926.

2. Bravo, C., Moshou, D., West, J., McCartney, A. and Ramon, H. 2003. Early Disease Detection in Wheat Fields Using Spectral Reflectance. *Biosyst. Eng.,* **84(2):** 137–145.

3. Chaerle, L., Lenk, S., Hagenbeek, D., Buschmann, C. and Van Der Straeten, D. 2007. Multicolor Fluorescence Imaging for Early Detection of the Hypersensitive Reaction to Tobacco Mosaic Virus. *J. Plant Physiol.,* **164(3):** 253–262.

4. Chaerle, L., Van Caeneghem, W., Messens, E., Lambers, H., van Montagu, M. and van der Straeten, D. 1999. Pre Symptomatic Visualization of Plant–Virus Interactions by Thermography. *Nature Bio. Technol.,* **17:** 813–816.

5. Horst, K. 1983. *Compendium of Rose Diseases.* The American Phytopathological Society, St. Paul, USA, 50 PP.

6. Lindenthal, M., Steiner, U., Dehne, H. W. and Oerke, E. C. 2005. Effect of Downy Mildew Development on Transpiration of Cucumber Leaves Visualized by Digital Infrared Thermography. *Phytopathol.,* **95(3):** 233-240.

7. Linde, M. and Shishkoff, N. 2003. Powdery Mildew. In: "*Encyclopedia of Rose Science*", (Eds.): Roberts, A., Debener, T. and Gudin, S. Academic Press, London, UK, PP. 158-165

8. Lins, E. C., Belasque Junior, J. and Marcassa, L.G. 2009. Detection of Citrus Canker in Citrus Plants Using Laser Induced Fluorescence Spectroscopy. *Precis. Agric.,* **10:** 319–330.

9. Macnish, A. J., Morris, K. L., De Theije, A., Mensink, M. G. J., Boerrigter, H. A. M., Reid, M. S., Jiang, C. Z. and Woltering, E. J. 2010. Sodium

Hypochlorite: A Promising Agent for Reducing *Botrytis cinerea* Infection on Rose Flowers. *Postharvest Biol. Technol.,* 58: 262-267.

10. Maghsoudi, H., Minaei, S., Ghobadian, B. and Masoudi, H. 2015. Ultrasonic Sensing of Pistachio Canopy for Low-Volume Precision Spraying. *Comput. Electron. Agr.,* **112:** 149-160.

11. Marcassa, L. G., Gasparoto, M. C. G., Belasque Junior, J., Lins, E. C., Dias Nunes, F., and Bagnato, V. S. 2006. Fluorescence Spectroscopy Applied to Orange Trees. *Laser Phys.,* **16(5):** 884–888.

12. Menessatti, P., Biocca, M., D'Andrea, S. and Pincu, M. 2008. Thermography to analyze distribution of agricultural sprayers. *QIRT J.,* **5:** 81-96.

13. Moltó, E., Martín, B. and Gutiérrez, A. 2001. PM–Power and Machinery: Design and Testing of an Automatic Machine for Spraying at a Constant Distance from the Tree Canopy. *J. Agr. Eng. Res.,* **77:** 379-384.

14. Moshou, D., Bravo, C., West, J., Wahlena, S. and McCartney, A. and Ramona, H. 2004. Automatic Detection of "Yellow Rust" in Wheat Using Reflectance Measurements and Neural Networks. *Comput. Electron. Agr.,* **44(3):** 173-188.

15. Moshou, D., Bravo, C., Oberti, R., West, J., Bodria, L., McCartney, A. and Ramon, H. 2005. Plant Disease Detection Based on Data Fusion of Hyper-Spectral and Multi-Spectral Fluorescence Imaging Using Kohonen Maps. *Real-Time Imaging,* **11(2):** 75–83.

16. Mostafaei Maynagh, B., Ghobadian, B., Jahannama, M. R. and Tavakoli Hashjin, T. 2009. Effect of Electrostatic Induction Parameters on Droplets Charging for Agricultural Application. *J. Agr. Sci. Tech.,* **11:** 249-257.

17. Oberti, R., Marchi, M., Tirelli, P., Calcante, A., Iriti, M. and Borghese, A. N. 2014. Automatic Detection of Powdery Mildew on Grapevine Leaves by Image Analysis: Optimal View-Angle Range to Increase the Sensitivity. *Comput. Electron. Agr.,* **104:** 1-8.

18. Oerke, E. C., Steiner, U., Dehne, H. W. and Lindenthal, M. 2006. Thermal Imaging of Cucumber Leaves Affected by Downy Mildew and Environmental Conditions. *J. Exp. Bot.,* **57:** 2121–2132.

19. Oerke, E. C., Fröhling, P. and Steiner, U. 2011. Thermographic Assessment of Scab Disease on Apple Leaves. *Precis. Agric.,* **12(5):** 699-715.

20. Polder, G., van der Heijden, G. W. A. M., van Doorn, J. and Baltissen, T. A. H. M. C. 2014. Automatic Detection of *Tulip Breaking Virus* (TBV) in Tulip Fields Using Machine Vision. *Biosyst. Eng.,* **117:** 35-42.

21. Prokop, M. and Kejklicek, R., 2002. Effect of Adjuvants on Spray Droplet Size of Water. *Res. Agri. Eng.,* **48:** 144–148.

22. Purcell, D. E., O'Shea, M. G., Johnson, R. A. and Kokot, S. 2009. Near-Infrared Spectroscopy for the Prediction of Disease Rating for Fiji Leaf Gall in Sugarcane Clones. *Appl. Spectrosc.,* **63(4):** 450–457.

23. Qin, J., Burks, T. F., Ritenour, M. A. and Bonn, W. G. 2009. Detection of Citrus Canker Using Hyperspectral Reflectance Imaging with Spectral Information Divergence. *J. Food Eng.,* **93(2):** 183–191.

24. Rowe, D. E., Malone, S. and Yates, Q. L. 2000. Automatic Greenhouse Spray System for Increased Safety and Flexibility. *Crop Sci.,* **40:** 1176-1179.

25. Rumpf, T., Mahlein, A. K., Steiner, U., Oerke, E. C., Dehne, H. W. and Plumer, L. 2010. Early Detection and Classification of Plant Diseases with Support Vector Machines Based on Hyperspectral Reflectance. *Comput. Electron. Agr.,* **74(1):** 91-99.

26. Sankaran, S, Ehsani, R. and Etxeberria, E. 2010a. Mid-Infrared Spectroscopy for Detection of Huanglongbing (Greening) in Citrus Leaves. *Talanta,* **83:** 574-581.

27. Sankaran, S., Mishra, A., Ehsani, R. and Davis, C. 2010b. A Review of Advanced Techniques for Detecting Plant Diseases. *Comput. Electron. Agr.,* **72(1):** 1-13.

28. Sayıncı, B., Bastaban, S. and Sanchez-Hermosilla, J. 2012. Determination of Optimal Spot Roundness Variation Interval for Droplet Size Analysis on Water Sensitive Paper. *J. Agr. Sci. Tech.,* **14:** 285-298

29. Shafri, H. Z. M. and Hamdan, N. 2009. Hyperspectral Imagery for Mapping Disease Infection in Oil Palm Plantation Using Vegetation Indices and Red Edge

Techniques. *Am. J. Appl. Sci.,* **6(6):** 1031–1035.

30. Spinelli, F., Noferini, M. and Costa, G. 2006. Near Infrared Spectroscopy (NIRs): Perspective of Fire Blight Detection in Asymptomatic Plant Material. *Proceeding in 10ᵗʰ International Workshop on Fire Blight, Acta Horticulturae,* **704:** 87–90.

31. Stoll, M., Schultz, H. R., Baecker, G. and Berkelmann-Loehnertz, B. 2008. Early Pathogen Detection under Different Water Status and the Assessment of Spray Application in Vineyards through the Use of Thermal Imagery. *Precis. Agric.,* **9:** 407–417.

32. Vadivambal, R. and Jayas, D. S. 2011. Applications of Thermal Imaging in Agriculture and Food Industry: A Review. *Food Bioprocess Tech*., **4:** 186-199.

33. Wang, M., Ling, N., Dong, X., Zhu, Y., Shen, Q. and Guo, S. 2012. Thermographic Visualization of Leaf Response in Cucumber Plants Infected with the Soil-Borne Pathogen *Fusarium oxysporum* f. sp. Cucumerinum. *Plant Physiol. Biochem.,* **61:** 153-161.

طراحی و ساخت سامانه تشخیص بیماری و سمپاشی موضعی گیاه رز براساس ترکیبی از تصاویر حرارتی و مرئی

س. مینایی، م. جعفری، ن. صفایی

چکیده

گیاه رز یکی از قدیمی ترین گل هایی است که کشت می شود و مشهورترین گل شاخه بریده دنیا می باشد و در معرض بیماری ها متعددی قرار دارد. بیماری های سفیدک پودری و کپک خاکستری دو نمونه از مهمترین بیماری‌های رز در کشت‌های گلخانه‌ای می باشند. تغییر در دمای برگ عمدتا ناشی از تغییر در تنفس گیاه در اثر تنش هایی از قبیل ابتلا به بیماری، تنش رطوبتی، یا تغییر در فیزیولوژی گیاه می باشد و این امکان وجود دارد که به صورت آنی و به روش دور سنجی با بهره گیری از تصاویر ترموگرافیک پایش گردند. در پژوهش حاضر، یک سامانه تشخیص و سمپاشی هوشمند برای شناسایی بیماریهای سفیدک پودری و کپک خاکستری با بهره گیری از ترکیب تصاویر حرارتی و مرئی طراحی و ساخته شد. سامانه شامل یک دوربین حرارتی و مرئی است که بر روی یک حامل C شکل نصب شده است. مجموعه تصویربرداری قادر است در طول ردیف کاشت حرکت کند و حول هر بوته گیاه بچرخد. علاوه بر آن یک سامانه خاص مکانی متشکل از یک شیر نیوماتیک کنترل جهت تحریک برقی، یک شیر نیوماتیک کنترل جهت تحریک بادی، یک رگولاتور فشار، یک مخزن تحت فشار، یک کمپرسور، یک شیر کنترل جریان دستی و یک افشانه، طراحی شده است. قطر میانه حجمی قطرات، درصد پوشش و عملکرد سامانه در سمپاشی مواضع مشخص شده، مورد ارزیابی قرار گرفت. آنالیز تصاویر حرارتی قبل و بعد از سمپاشی نشان داد که شاخصی مانند میانه دمایی می توانند به خوبی نشان دهنده درصد پوشش و یکنواختی پاشش باشند.